Prepared for submission to JHEP

Cavendish-HEP-15/11
DESY 15-169
November 10, 2015

Probing the top-quark width through ratios of resonance contributions of $e^+e^- \to W^+W^-b\bar{b}$

Stefan Liebler,[a] **Gudrid Moortgat-Pick**[ab] **and Andrew S. Papanastasiou**[ac]

[a] *DESY, Deutsches Elektronen-Synchrotron, Notkestraße 85,D-22607 Hamburg, Germany*
[b] *II. Institut für Theoretische Physik, Universität Hamburg, Luruper Chaussee 149, 22761 Hamburg, Germany*
[c] *Cavendish Laboratory, University of Cambridge, J.J. Thomson Avenue, CB3 0HE, Cambridge, UK*

E-mail: stefan.liebler@desy.de, gudrid.moortgat-pick@desy.de, andrewp@hep.phy.cam.ac.uk

Abstract: We exploit offshell regions in the process $e^+e^- \to W^+W^-b\bar{b}$ to gain access to the top-quark width. Working at next-to-leading order in QCD we show that carefully selected ratios of offshell regions to onshell regions in the reconstructed top and antitop invariant mass spectra are, *independently* of the coupling g_{tbW}, sensitive to the top-quark width. We explore this approach for different centre of mass energies and initial-state beam polarisations at e^+e^- colliders and briefly comment on the applicability of this method for a measurement of the top-quark width at the LHC.

Contents

1 Introduction

After the spectacular discovery of a signal in the Higgs searches at the Large Hadron Collider (LHC) [1, 2] a future linear collider, such as the International Linear Collider [3–7], provides rich and exciting physics prospects in the context of the Standard Model (SM) of particle physics and of course beyond. Aside from the detailed properties of the Higgs boson, which can be measured with high accuracy at a linear collider, the precise determination of top-quark properties is also of high priority, as these may also provide an interesting window to new physics. For recent reviews of linear collider physics we refer to refs. [8, 9] and a comprehensive review on top-quark physics at a linear collider can be found within refs. [10, 11].

It is well-known that the precise measurement of many top-quark properties, including that of a well-defined mass parameter, is optimally performed by studying the production of a top-quark pair near threshold, that is at a centre of mass $\sqrt{s} \sim 2m_t \sim 350\,\text{GeV}$ where the two top quarks are produced almost at rest and show strong binding effects. However, it is not the purpose of this paper to revisit this phase space region and we refer to refs. [8, 9] and the plethora of references therein for details and insights. A linear collider is likely to initially operate at a higher centre of mass energy $\sqrt{s} \geq 500\,\text{GeV}$ [12], where top-quark pairs are produced in the continuum rather than at rest. There are a number of good reasons to start a linear collider run at a higher centre of mass energy including: making a measurement of the top-quark Yukawa coupling possible early on, recording of Higgsstrahlung and vector-boson fusion events and thus determining the couplings of the Higgs boson to heavy gauge bosons and, of course, better probing regions of phase space where new physics is more likely to appear. Therefore, despite the fact that a run at threshold will allow the extraction of theoretically more consistent and experimentally easier to measure top-quark properties, it is important to explore what possibilities for precise measurements of top-quark properties are offered by the continuum region.

Top-quark production in the continuum in e^+e^- collisions has and continues to be a subject of much theoretical attention. Onshell top-quark pair-production in the continuum is now known at next-to-next-to-leading order (NNLO) in QCD [13–23]. Relaxing the assumption of stable top quarks, top-pair production and decay in e^+e^- collisions has been studied in the narrow-width approximation in ref. [24]. The full process $e^+e^- \to W^+W^-b\bar{b}$, in which intermediate top quarks can have arbitrary offshellness was first computed at next-to-leading order (NLO) in ref. [25] and recently revisited in refs. [26, 27]. Leading order (LO) predictions for $e^+e^- \to 6$ fermions can be found in [28]. A discussion of top-quark production with unstable top quarks in the continuum and in the regime of boosted tops, using a tower of effective field theories was provided in refs. [29, 30]. The latter compute the double differential cross section with respect to the invariant masses of the two top quarks to next-to-leading-log, and show that in such a regime a well-defined mass parameter can, in principle, be determined with an accuracy of better than $\mathcal{O}(\Lambda_{\text{QCD}})$.

In this work we explore the idea of obtaining the top-quark width, Γ_t, by exploiting the different resonance regions in the reconstructed top and antitop invariant mass distributions that are present in the process $e^+e^- \to W^+W^-b\bar{b}$. Top-pair and single top production co-

exist in this full process and contributions to the different regions can be identified as double-resonant or single-resonant top-quark production, which intrinsically differ in their dependence on Γ_t. For our investigation we simulate the fully-differential process using MadGraph5_aMC@NLO [31] at LO and NLO in QCD and emphasise that the full set of diagrams for $e^+e^- \to W^+W^-b\bar{b}$ (i.e. those with two, one and no intermediate top-quark propagators) is included in the calculation.

Our paper is organized as follows: In the remainder of section 1, we motivate our approach by showing an analogy to the determination of the Higgs boson width from offshell regions and later transfer the idea to the case of the top-quark width, for which the current theoretical and experimental knowledge is also briefly reviewed. In section 2 we discuss the process $e^+e^- \to W^+W^-b\bar{b}$ at NLO QCD, including our numerical setup and details on relevant distributions. We also provide a detailed examination of the reconstructed top-quark mass distribution, thus gaining insight into the structure of the different resonance regions of this process. In section 3 we show how the method for the Higgs boson is modified in the case of a pair of unstable top quarks. We apply this method to $e^+e^- \to W^+W^-b\bar{b}$ and illustrate how it enables one to gain access to the top-quark width. We additionally investigate the potential for enhanced sensitivities by exploiting polarised beams or higher centre of mass energies. Finally, we also discuss how our analysis may be improved in future studies and comment on the applicability of our method at the LHC. We end with our conclusions in section 4.

1.1 Offshell regions and the Higgs boson width

After the discovery of a SM-like Higgs boson at 125 GeV, offshell contributions in the decay of the SM Higgs into a pair of vector bosons (V) were found to be sizeable [32–34]. Offshell region measurements have offered an opportunity to indirectly constrain the width of the Higgs boson at the LHC via the method proposed in refs. [35–37]. The key idea is that the ratio of offshell to onshell cross section measurements is sensitive to the total Higgs width, Γ_H. This can be inferred by examining how the cross sections in the different regions scale with the couplings involved in Higgs production and decay and how they scale with Γ_H. The onshell cross section receives contributions from phase space where the invariant mass of the vector-boson pair is close to the Higgs boson pole mass, $M(V,V) \sim m_H$, and scales as $\sigma^{\text{on}}_{VV} \sim g^2_{\text{on}}\Gamma_H^{-1}$, where g_{on} encodes all couplings involved in Higgs production and decay. In contrast, events with $M(V,V) \gg m_H$ contribute to the offshell cross section, which scales as g^2_{off}, i.e. it is independent of the Higgs boson width Γ_H.

Under the assumption that the couplings in the offshell region g_{off} can be related to those in the onshell region g_{on} then an extraction of the width is possible simply by relating the on- and offshell signal strength. For details in case of e^+e^- collisions we refer to ref. [38], where offshell effects in Higgs production at a linear collider were discussed. It must be emphasised that the extracted bound on the Higgs width ought to be taken with some care as it is based on an assumed relation between on- and offshell couplings, namely that the onshell and offshell κ factors are equal.[1] The latter relation can be severely affected by

[1] For a definition of the κ-factors framework, we refer to refs. [39, 40].

Beyond-the-Standard Model (BSM) physics as discussed in refs. [41–44] for the LHC and in ref. [38] for a linear collider.

1.2 Offshell regions and the top-quark width

In section 2 and section 3 we investigate whether a similar procedure of relating cross sections in different kinematic regimes can be applied to the case of top-quark production to infer the total width of the top quark, Γ_t. For this purpose we consider the process $e^+e^- \to W^+W^-b\bar{b}$. This is the relevant final state for the top-quark pair production process where the decay of the tops is included. However, the full perturbative calculation we work with contains single resonant and non resonant contributions in addition to the usual double-resonant contributions and also includes full finite-top-width effects. We consider the various resonance regions present in the double differential cross section

$$\frac{d^2\sigma^{e^+e^-\to W^+W^-b\bar{b}}}{dM(W^+,J_b)\,dM(W^-,J_{\bar{b}})}\,, \tag{1.1}$$

where $M(W^+,J_b)$ and $M(W^-,J_{\bar{b}})$ are the top and antitop masses reconstructed through the W-bosons and $b/\bar{b}$-flavoured jets, $J_b/J_{\bar{b}}$, present in the final state. The different resonance regions are influenced to varying degrees by all of the double resonant ('top-pair'), single resonant ('single top') and non resonant ('no top') subprocesses to $e^+e^- \to W^+W^-b\bar{b}$.

There are a few differences between the method used to place bounds on the Higgs boson width and the one we propose here to become sensitive to Γ_t. Firstly, unlike in the case of the Higgs boson, we work in a limited kinematic range rather close to the top quark resonance peaks $M(W^+,J_b),\ M(W^-,J_{\bar{b}}) \sim m_t \pm 50\,\text{GeV}$. In this range the influence of possible 'high-mass' BSM contributions is therefore limited and we can safely treat the involved couplings, most prominently the coupling of the top-quark to the W boson and the bottom quark, g_{tbW}, as constants.[2] Additionally, we only consider variations of the top-quark width up to $\pm 20\%$ of the SM value, whereas in the case of the Higgs boson the experimental sensitivity corresponds to a width which is multiple times the SM Higgs boson width. Another difference is that here we consider ratios of cross sections in single and double resonant regions which receive contributions from phase-space where one or two reconstructed top quarks are 'nearly' onshell. In the Higgs boson case however, contributions from onshell (resonant) Higgs boson production are compared with far-offshell Higgs boson production. We discuss this in detail a little later.

1.3 Status and prospects of top-quark width measurements

Before proceeding to a detailed description of our proposed method, we first comment on the theoretical knowledge of Γ_t and its experimental measurement. At LO in the SM the top-quark width is dominated by the decay into the W boson and a b quark, which depends on the g_{tbW}-coupling as

$$\Gamma(t\to Wb) = \left(\frac{g_{tbW}}{g}\right)^2 \frac{G_\mu m_t^3}{8\sqrt{2}\pi}\left(1-\frac{m_W^2}{m_t^2}\right)^2\left(1+\frac{2m_W^2}{m_t^2}\right)\,, \tag{1.2}$$

[2] Therefore, in contrast to the case of Higgs boson at the LHC, the assumed relation between onshell and offshell couplings is a much weaker one in the setup we consider here.

where g denotes the electroweak coupling of $\mathrm{SU}(2)_L$, G_μ Fermi's constant and m_t and m_W the top-quark mass and W boson mass respectively (for simplicity we have set the bottom-quark mass to zero above). Apart from NLO QCD corrections [45–47] higher order QCD as well as electroweak corrections to $\Gamma(t \to Wb)$ are known [48–53]. In the SM g_{tbW} can be written as gV_{tb} where V_{tb} is the corresponding CKM matrix element. Since the branching fraction to a W boson and a b quark is almost 100%, the total top-quark width is almost linearly dependent on g^2_{tbW}.

Now we give a short summary of current measurements of Γ_t. Its value can be deduced from the measurement of the branching ratio $\mathrm{BR}(t \to Wb)$ together with the partial decay width $\Gamma(t \to Wb)$. The former can be accessed through the ratio $R = \mathrm{BR}(t \to Wb)/\sum_{q=d,s,b} \mathrm{BR}(t \to Wq)$ measurable from top-pair production, which, being experimentally compatible with $R = 1$ [54], points towards $\mathrm{BR}(t \to Wb) \sim 100\%$. This measurement also implies strong bounds on non-SM top-quark decays such as $t \to H^+ b$ [54]. The partial decay width can be indirectly determined through eq. (1.2) by a measurement of g_{tbW}, on which we subsequently focus. Whereas g is known with great precision [54], the CKM matrix element can either be deduced from a global fit $V_{tb} = 0.99914 \pm 0.00005$ [54] assuming unitarity of the CKM matrix or from single top quark production (whereas top-quark pair production is insensitive to g_{tbW}). The average of the single top quark production cross section obtained by the Tevatron and the LHC experiments leads to $|V_{tb}| = 1.021 \pm 0.032$ [54], which can be used to indirectly extract the top-quark width to an accuracy of order 100 MeV. The coupling g_{tbW} can be altered in models beyond the SM – we direct the interested reader to refs. [55, 56] for concrete examples in the context of a 2-Higgs-Doublet Model, the Minimal Supersymmetric Standard Model or top-color assisted Technicolor. Their effects are most dominant in the left-handed part of the coupling g_{tbW} and are in the range of a few percent. We point out that though g_{tbW} may differ from its SM value, this does not affect the validity of the assumption of equal on- and offshell couplings discussed in section 1.2. For completeness we note that CDF also obtained direct bounds on Γ_t, specifically, $1.10\,\mathrm{GeV} < \Gamma_t < 4.05\,\mathrm{GeV}$ at 68% confidence level [57], from template fits of the reconstructed top masses in $t\bar{t}$ events.

At a linear collider Γ_t can be directly deduced from top-quark pair production at threshold (see [8] and references therein). The dependence of the cross section on Γ_t is nicely illustrated in ref. [58]. Furthermore, the forward-backward asymmetry in $e^+e^- \to t\bar{t}$ near threshold shows a clear dependence on Γ_t [10]. Refs. [59–61] report a projected accuracy of $20 - 30\,\mathrm{MeV}$ on Γ_t from top-quark pair production measurements at threshold. In the continuum, due to the fine-resolution detectors and the cleaner environment at a linear collider, performing fits of the invariant-mass lineshape (reconstructed via the decay products of the top quark) provides a realistic method to precisely determine the top-quark width. We will comment on this extraction method in section 2.4, however we highlight that refs. [61, 62] estimate that, using reconstruction of the invariant mass at a linear collider, Γ_t can be determined with a precision of $60 - 220\,\mathrm{MeV}$ for $\sqrt{s} = 500\,\mathrm{GeV}$ and an integrated luminosity of $100\,\mathrm{fb}^{-1}$.

As we will describe in the following sections, taking carefully chosen ratios of measurements of offshell and onshell regions (these will be quantified below) can also provide access

to the top-quark width. The ratios are independent of explicit powers of the coupling g_{tbW}, in principle allowing one to disentangle the coupling g_{tbW} and the width Γ_t.

2 $e^+e^- \to W^+W^-b\bar{b}$ at NLO in QCD

The process we consider here is

$$e^+e^- \to W^+\,W^-\,J_b\,J_{\bar{b}} + X\,. \tag{2.1}$$

Specifically, J_b and $J_{\bar{b}}$ are bottom-flavoured jets containing at least a b or a $\bar{b}$ parton respectively. The presence of top quarks is inferred by a reconstruction b-flavoured jets and W-bosons (the latter also determined via their decay products, leptons or jets, experimentally). The process is generated at fixed-order (LO and NLO-QCD) using the MadGraph5_aMC@NLO code [31] which uses MadLoop [63] for the evaluation of the one-loop matrix element and MadFKS [64] (based on FKS subtraction [65]) to handle the singular regions of the real corrections. Additionally, the complex-mass scheme [66, 67] is employed to consistently introduce the top-quark width. The bottom quark is considered to be stable and its mass is renormalized onshell. We note that this process was first studied in ref. [25] and was briefly discussed in ref. [26]. Recently the authors of the WHIZARD Event Generator [68, 69] have also investigated this process at NLO-QCD in ref. [27]. The Feynman diagrams contributing to this process include double, single and non resonant diagrams and at the amplitude-squared level all of these interfere with each other. Tree-level examples of these are shown in figure 1.

The inclusive $W^+W^-b\bar{b}$ cross section is dominated by the double resonant $t\bar{t}$ contributions, namely, contributions from diagrams such as diagram (a) in figure 1 which contains two resonant top-quark propagators. This is particularly the case near threshold. However, at centre of mass energies above threshold the relative contribution of single and non-resonant terms (arising from diagrams such as (b) & (c) and (d) respectively of figure 1) increases [70]. Single and non-resonant contributions also become very relevant below threshold where the production of a resonant $t\bar{t}$ pair becomes kinematically suppressed, as discussed in ref. [55]. Therefore, both in the continuum as well as below threshold, having a faithful description of the full $W^+W^-b\bar{b}$ final state is of great importance.

As mentioned above, the complex-mass scheme is used to consistently introduce a complex mass at the Lagrangian level. This renormalization procedure replaces the bare top-quark mass, $m_{t,0}$ by a renormalized mass, μ_t, and a counter-term, $\delta\mu_t$, both of which are complex,

$$m_{t,0} = \mu_t + \delta\mu_t\,, \tag{2.2}$$

where $\mu_t^2 = m_t^2 - i m_t\Gamma_t$. In this scheme the value of the top-quark width is considered as an input and the counter-term is chosen such that μ_t^2 corresponds to the pole of the renormalized top-quark propagator. Formally, this means that if one uses fixed-order predictions with the complex-mass scheme to extract the top-quark mass, then the mass parameter one is sensitive to is the pole mass, defined as $m_t^2 = \mathrm{Re}[\mu_t^2]$. Accordingly, the employed top-quark width is defined via $m_t\Gamma_t = -\mathrm{Im}[\mu_t^2]$. The complex-mass scheme has already

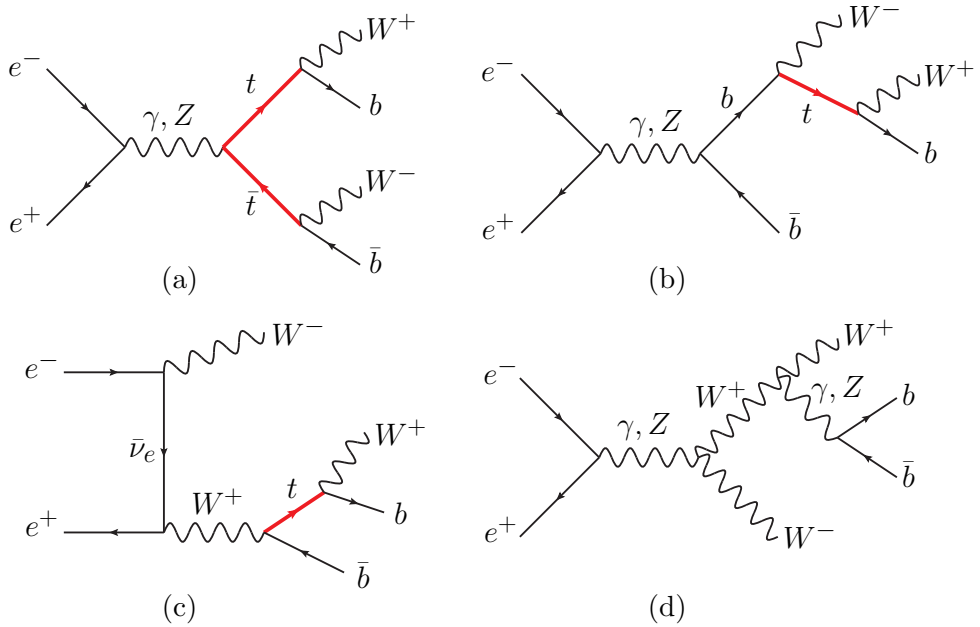

Figure 1. Sample tree-level Feynman diagrams contributing to the full LO $e^+e^- \to W^+W^-b\bar{b}$ amplitude. These include (a) double resonant, (b) & (c) single resonant and (d) non-resonant diagrams.

been used to compute NLO predictions for a number of processes involving unstable top quarks at hadron colliders [71–76].

2.1 Setup

We summarize the parameter and analysis setup used throughout this paper in this subsection. The results we present, with the exception of the discussion in section 3.2.2, are for a centre of mass energy of $\sqrt{s} = 500$ GeV. We begin our investigation for unpolarised initial-state electrons and positrons, but extend our analyses to polarised beams in section 3.2.1. The numerical values of the relevant parameters used to produce our results are found in table 1. We use eq. (1.2), including bottom-quark mass effects, to obtain our numerical input value for the LO top-quark width and the result of ref. [46] to calculate the NLO top-quark width. In addition, we note that the assumption of a diagonal CKM matrix is made, namely we take $V_{tb} = 1$. The effect of a finite width of the W-boson is negligible for the observables we consider here, in particular since intermediate W-boson propagators are forced to be offshell by kinematics. At NLO QCD the cross section develops a dependence on the renormalization scale μ_R (see section 2.2) and we employ a central scale choice of $\mu_R = m_t$ – a standard scale choice for the study of the $t\bar{t}$ process in e^+e^- collisions. As we will see later, the inclusive cross section is very mildly dependent on this scale.[3]

[3]In the respective hadron-collider process, $pp \to W^+W^-b\bar{b}$ choosing appropriate renormalization and factorization scales is not as simple, particularly when trying to describe the single resonant contribution of the cross section. This is due to the different underlying subprocesses governing the double and single resonant regions. For an in-depth discussion on this and on a possible scale-setting procedure for pp collisions we refer the reader to ref. [76].

Parameter Setup			
$m_t = 173.2$ GeV	$m_b = 4.75$ GeV	$m_W = 80.385$ GeV	$m_Z = 91.1886$ GeV
$m_H = 125$ GeV	$\Gamma_Z = 2.505$ GeV	$\Gamma_H = 4.21$ MeV	$G_\mu = 1.1664 \times 10^{-5}\text{GeV}^{-2}$

Table 1. Parameter choices.

Partons in the final state are clustered into (a maximum of three) jets using the k_t-algorithm, as implemented in `fastjet` [77]. Tagging jets as b, $\bar{b}$ or light jets is done using the flavour information of partons in each jet that is available in our parton-level analysis. For most results we use a jet radius of $R_{\text{jet}} = 0.5$. However, since the different combinations through which gluon radiation can be clustered play an important role in the structure of the invariant-mass distributions (see below), the jet-radius parameter, R_{jet}, is varied (enlarged) in order to better understand the extent to which this affects m_t or Γ_t extractions. Minimal cuts of $p_T(J_b), p_T(J_{\bar{b}}) > 10$ GeV and $|\eta(J_b)|, |\eta(J_{\bar{b}})| < 4.5$ have been applied to the b-jets to define a typical fiducial region. This means that phase space points for which the b and $\bar{b}$ partons are combined into the same jet are dropped in our analysis.

2.2 Inclusive and differential results

We first briefly discuss the dependence the cross sections have on the renormalization scale μ_R. We note that at LO, since the amplitudes do not depend on α_s there is no dependence on μ_R. Of course, the NLO cross section picks up a dependence on μ_R and in order to study this dependence we use a fixed renormalization scale $\mu_R = \xi m_t$ and vary $\xi \in [0.1, 5]$. As illustrated in figure 2, both the fully-inclusive cross section as well as the fiducial cross section, defined according to the analysis cuts of section 2.1, only have a mild dependence on μ_R. We note however that the NLO corrections themselves are important, enhancing the LO numbers by around $10 - 12\,\%$.

In figure 3 we show two example distributions, (a) the transverse momentum of the reconstructed top quark, $p_T(W^+, J_b)$ and (b) the transverse momentum of the W^+W^- pair, $p_T(W^+, W^-)$. This is done to highlight that the code allows for the study of any infrared-safe differential observable that can be constructed using the full final state. While it is not the purpose of this paper to discuss the effects of NLO corrections to the $e^+e^- \to W^+W^-b\bar{b}$ process, we indicate in the lower panels of figure 3 (a) and (b) that the NLO corrections do, for some observables, lead to non-constant differential K-factors. Offshell and non resonant effects will also play an important role in the tails of certain observables such as those in figure 3. However, to quantify the role of such effects would require (at least) a comparison with the process in the narrow-width approximation, $e^+e^- \to t\bar{t} \to W^+W^-b\bar{b}$, at NLO (including NLO corrections to both production at decay subprocesses), which is beyond the scope of this paper. Such comparisons at NLO for hadron-collider processes involving unstable top quarks can be found in refs. [72–74, 76, 78–80].

2.3 Invariant mass of reconstructed top quarks

We now examine the distribution for $M(W^+, J_b)$, explaining the structure behind the shapes of the curves at LO and NLO. A better understanding of this distribution will be

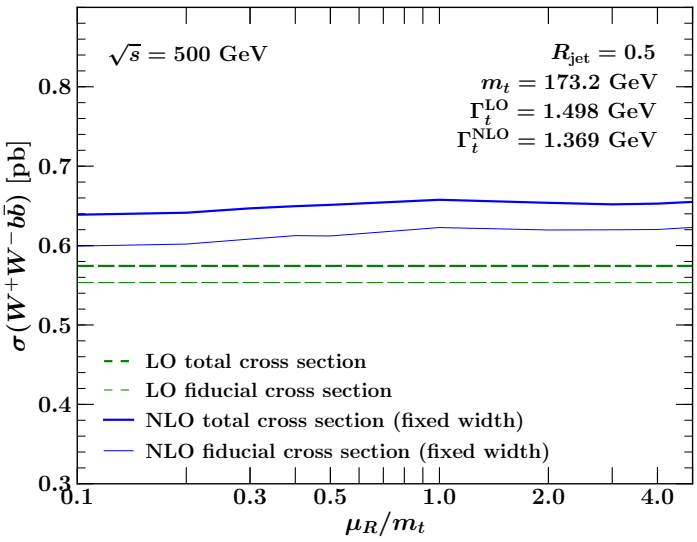

Figure 2. Dependence on renormalization scale of inclusive (thick solid curves) and fiducial (thin solid curves) cross sections. The dashed green curves indicate the LO cross sections whist the solid blue curves show the μ_R-dependence of the NLO cross sections.

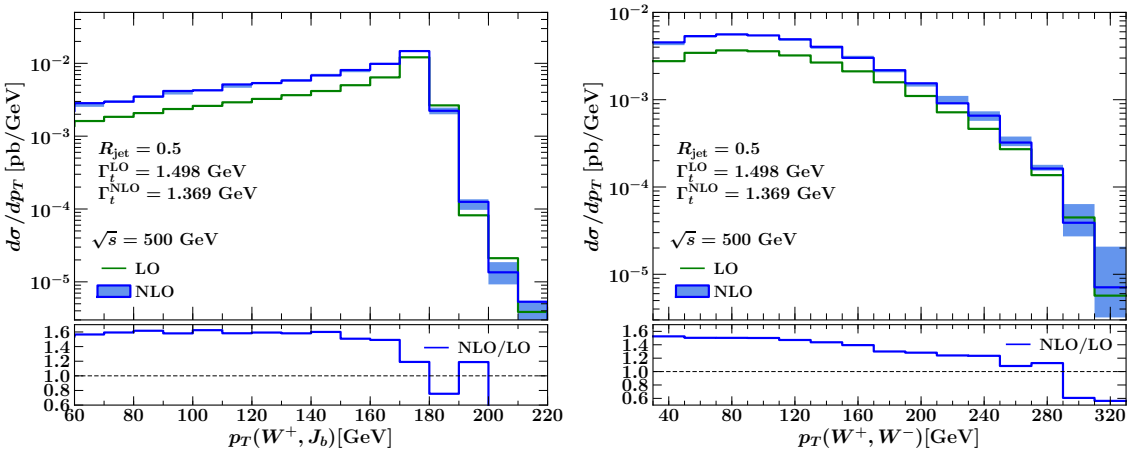

Figure 3. Distributions for the transverse momentum of (a) the reconstructed top quark, $p_T(W^+, J_b)$ and (b) the W^+W^--pair, $p_T(W^+, W^-)$. Upper panels: the green curves indicate the LO distributions whilst the blue band shows the NLO result, where the band is obtained by varying the renormalisation scale in the range $\mu_R \in [m_t/2, 2m_t]$. Lower panels: the blue solid curves indicate the differential K-factor.

key to explaining the patterns in the results we present in section 2.4 and section 3.

In figure 4 we plot the invariant-mass distribution of the reconstructed top quark, $M(W^+, J_b)$ at LO in green and at NLO in blue, for $R_{\rm jet} = 0.5$ in the ranges (a) $[120, 220]$ GeV and (b) $[162, 182]$ GeV. The shape of the LO curve around the peak, where the cross section is dominated by diagrams involving intermediate top quarks, is that of a standard

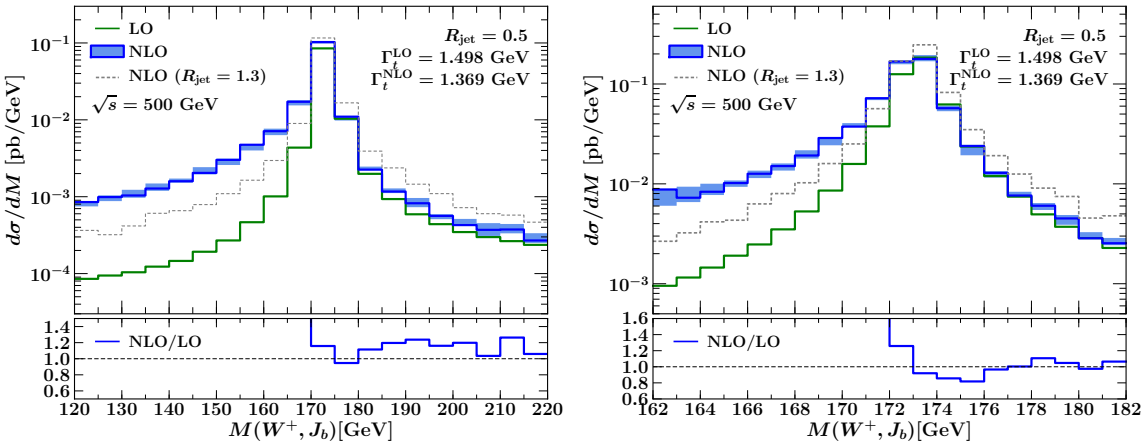

Figure 4. Distributions for the reconstructed top quark mass, $M(W^+, J_b)$, in the range (a) $M(W^+, J_b) \in [120, 220]$ GeV and (b) $M(W^+, J_b) \in [162, 182]$ GeV. Upper panels: the green curves indicate the LO distributions whilst the blue band shows the NLO result, where the band is obtained by varying the renormalisation scale in the range $\mu_R \in [m_t/2, 2m_t]$. The green and blue solid curves show the results for a jet radius of $R_{\rm jet} = 0.5$ whilst the dashed gray curve shows the NLO distribution for $R_{\rm jet} = 1.3$. Lower panels: the blue solid curves indicate the differential K-factor.

Breit-Wigner distribution. Moving out towards the tails of the distributions, non resonant diagrams contribute to distort this shape. Going from LO to NLO one observes large differences between the LO and NLO results, with the LO curve lying outside the NLO scale uncertainty band, particularly for the region $M(W^+, J_b) < m_t$.

To understand the reasons behind these large differences it is instructive to first consider the case of production and decay of a single onshell top quark. In this case at LO it is always the case that the intermediate top-quark momentum is $p_t = p_W + p_b$, as illustrated in figure 5(a), and all the cross section sits at $M(W^+, J_b) = m_t$. NLO virtual corrections to this process do not change the virtuality of the reconstructed invariant mass, namely for virtual contributions we still have $M(W^+, J_b) = m_t$. In contrast, NLO real corrections can change the virtuality of the reconstructed top. In the onshell approximation for the real-emission contributions we can either have that the intermediate top momentum is equal to $p_t = p_W + p_b$, for the case of an emission from the production subprocess, or that the top momentum is equal to $p_t = p_W + p_b + p_g$, in the case of an emission from the top-decay subprocess. These two cases are illustrated schematically in figure 5 (b) and (c) respectively.

When the momenta for the b and g momenta are fed to the jet algorithm the gluon momentum is either clustered together with or separately from the b-parton. In the case where there is an emission from the production subprocess, then either the gluon is clustered with the b-parton, thus increasing the reconstructed mass $M(W^+, J_b) > m_t$, or the gluon is not clustered with the b-parton, and the invariant mass remains at $M(W^+, J_b) = m_t$. In the case of a gluon emission from the decay subprocess, then either the gluon is clustered

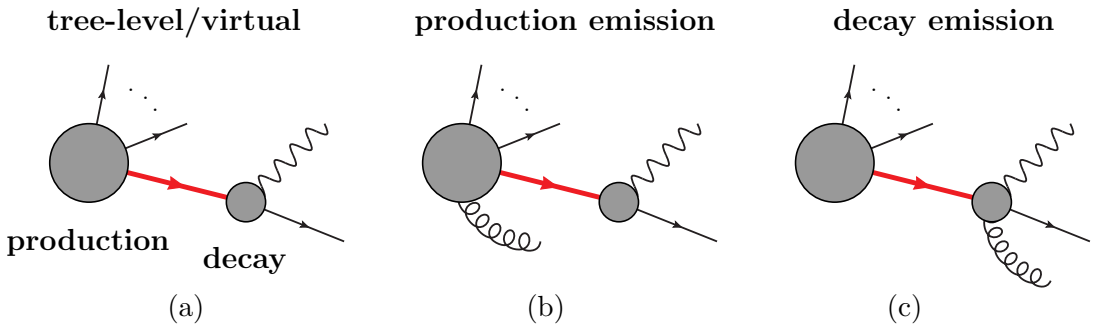

Figure 5. Schematic diagrams indicating structure of amplitudes in limit of onshell top quark production and decay.

together with the b-parton meaning that the invariant mass remains at $M(W^+, J_b) = m_t$, or the gluon is clustered separately from the b-parton resulting in $M(W^+, J_b) < m_t$. Since the contributions that change the virtuality of the reconstructed top quark can only arise from real corrections at NLO (in the case of the narrow-width approximation that we consider here) they are positive contributions. In the case of onshell top production and decay this leads to tails forming away from the peak at $M(W^+, J_b) = m_t$.

Having understood the structure in the case of onshell top production, we move to the case of interest, namely offshell top-pair production, or $W^+W^-b\bar{b}$ production. Since intermediate top quarks are now generically offshell and additionally non resonant terms contribute, the distribution for the invariant mass receives contributions both above and below $M(W^+, J_b) = m_t$ starting at LO. The bulk of the cross section does still lie in or near the bin containing the point $M(W^+, J_b) = m_t$, indicating that the resonant contributions are dominant. For this reason, the one-loop virtual corrections also do not change the structure of the LO curve significantly, even though there are many contributing corrections in addition to the one-loop corrections to the production and decay subprocesses that we considered in our toy-setup.

On the other hand the real corrections, as in the onshell case, can and do modify the LO shape of the reconstructed mass and the underlying reasons for this are precisely the same as those discussed in the case of an onshell top quark. Firstly, a positive contribution is expected for $M(W^+, J_b) < m_t$, due to emissions from an offshell resonant top, where $(p_W + p_b + p_g)^2 \sim m_t^2$, which are *not* captured in the b-jet. Secondly a similar positive contribution is expected in the region $M(W^+, J_b) > m_t$, due to emissions that do not change the virtuality of the intermediate resonant top, i.e. where $(p_W + p_b)^2 \sim m_t^2$, but which are however captured inside the b-jet.

From the above discussion it is clear that precisely how the distribution for $M(W^+, J_b)$ is affected by the NLO corrections is dependent on how real radiation is clustered into jets and in particular the radius of the jets. In figure 4 we also show the NLO distribution for $M(W^+, J_b)$ for $R_{\text{jet}} = 1.3$ (typically used in many linear collider top-quark analyses), where we see that the effect of increasing the jet radius moves the NLO curve down for $M(W^+, J_b) < m_t$ and up for $M(W^+, J_b) > m_t$. This is due to the fact that with a wider

jet radius, on the one hand, one loses the gluon radiated from the top-decay subprocess outside the jet (leading to the lowering of the tail $M(W^+, J_b) < m_t$) less often, but on the other hand, more frequently captures radiation from the top-production subprocess or elsewhere into the b-jet (resulting in the increase of the tail $M(W^+, J_b) > m_t$).

Finally, we mention that given the impact of a single gluon emission on the shape of the distribution, it is evident that multiple gluon emissions during the parton-showering stage of a full event simulation will further affect the shape. In particular, parton-showering is expected to further broaden the lineshape of the reconstructed top quarks and is certainly an effect worth additional investigation (though lies beyond the scope of this work).

2.4 Uncertainty on m_t and Γ_t extraction from kinematic reconstruction

In this subsection we briefly comment on a method commonly used to extract both the top-quark mass and width in the continuum. This consists of a simple fit of a Breit-Wigner (BW) function to the reconstructed mass peak $M(W^+, J_b)$ or $M(W^-, J_{\bar{b}})$ (see for example [61]). The method is usually applied to samples of simulated events where the underlying hard process is onshell top-quark pair production $e^+e^- \to t\bar{t}$. These events are then supplemented with the corresponding LO decay of the top quarks by a parton shower and offshellness is inserted through a BW-smearing of the virtuality of the intermediate top-quarks. Since the exact shapes for the reconstructed masses can be predicted at both LO and NLO, and these are *not* exact BW functions, it is of interest to investigate to what extent fitting a BW function is a suitable method for extracting m_t and Γ_t or whether significant errors are introduced in doing so. Here we focus on the extraction of the top-quark mass and width using the full process $e^+e^- \to W^+W^-b\bar{b}$ at NLO in QCD. Gluon emission at NLO in general broadens the peak, in particular at the invariant masses below the peak, and can thus potentially pull the extracted mass towards a smaller central value. As discussed earlier, the shape of the reconstructed mass shows a strong dependence on the jet radius used in the definition of b-jets.

We start with input values of $m_t = 173.2$ GeV and $\Gamma_t = 1.369$ GeV as input to MadGraph5_aMC@NLO, using the latter to generate a distribution for $M(W^+, J_b)$ for $R_{\text{jet}} = \{0.5, 0.9, 1.3\}$. We then fit a BW function to these distributions extracting m_t^{meas} and Γ_t^{meas} as those parameters for which the BW function best models the distribution. This is done using a least-squares method and the goodness-of-fit is comparable (and very good) in all three cases. Specifically, the standard deviation for the extracted values of m_t^{meas} and Γ_t^{meas} is always below 60 MeV. We note that we have performed this simple exercise assuming perfect $b/\bar{b}$-jet tagging and reconstruction of W^+ and W^-. For $R_{\text{jet}} = 0.5$ we extract a mass and width of $m_t^{\text{meas}} = 173.00$ GeV and $\Gamma_t^{\text{meas}} = 1.92$ GeV, for $R_{\text{jet}} = 0.9$ we find $m_t^{\text{meas}} = 173.14$ GeV and $\Gamma_t^{\text{meas}} = 1.55$ GeV and for $R_{\text{jet}} = 1.3$ we find $m_t^{\text{meas}} = 173.20$ GeV and $\Gamma_t^{\text{meas}} = 1.30$ GeV. We see that with increasing R_{jet} the extracted values for the mass and width approach the input values. This is due to the fact that with increasing R_{jet}, gluon radiation from intermediate top decays is more likely to be clustered in a way that least distorts the LO BW shape near the resonance peak, as discussed in section 2.3. In figure 6 we show the best-fit BW lineshapes as a function of the jet radius

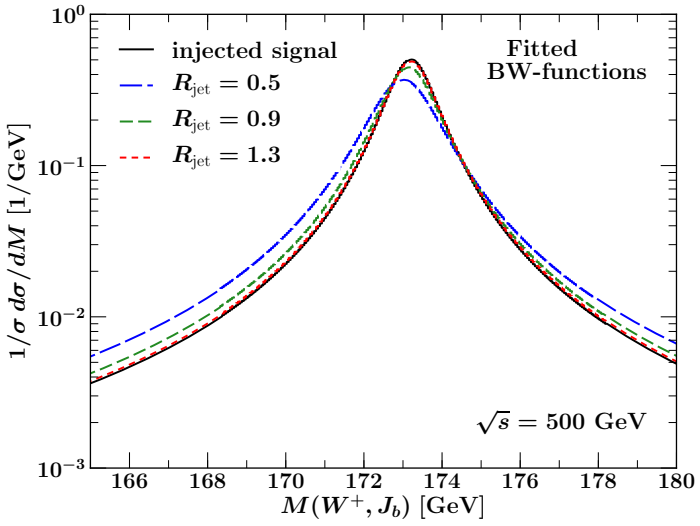

Figure 6. Reconstructed Breit-Wigner shapes as a function of $M(W^+, J_b)$ for different employed values of the jet radius. The curves are normalized to the total inclusive cross section. The injected signal corresponds to the black, solid curve.

(in dashed blue, green and red) as well as the BW lineshape corresponding to the original input values used (in solid black).

To summarize, we would like to point out that a perturbative uncertainty of up to a few hundred MeV exists in the extraction of Γ_t using a fit of a BW function (which essentially models the LO invariant mass) to an NLO $M(W^+, J_b)$ distribution. The size of this depends on the jet radius and should be taken into account when performing such extractions. The origin of the uncertainty appears to be predominantly due to gluon emissions distorting the LO lineshapes. This analysis is performed at fixed-order and despite the fact that parton showers capture some of the effects of hard radiation in the top-quark decay (and thus may decrease this uncertainty), we believe that the systematic error on extracting Γ_t examined here will very likely remain until an extraction using the full NLO plus parton shower predictions of $e^+e^- \to W^+W^-b\bar{b}$ become available. Until these new tools are utilised it should be kept in mind that template or BW-fitting extractions of the width based on simulations using LO top-quark decays (such as those performed for example in refs. [61, 62]) ought to include a potentially important systematic error due to these missing higher-order effects. We note that there is a corresponding, but smaller, uncertainty of about 200 MeV in the extraction of m_t.

We point out that it is known that the BW lineshape is additionally distorted by non-perturbative QCD effects. As explained in refs. [29, 30], these can shift the extracted top-quark mass and width to larger values; an effect that increases with the centre of mass energy. Control of such effects could be achieved through their encoding in universal soft functions.

3 Sensitivity of offshell regions to the top-quark width

In this section we investigate the extent to which the idea of using the cross section in offshell regions to probe or place bounds on the total width can be applied to top-pair production when measurements on the full final state of $W^+W^-b\bar{b}$ are made. This possibility, which does not depend on fitting a particular functional form to a lineshape, is interesting to explore as an alternative handle on Γ_t in the continuum. Furthermore, the different choices one has in setting up this method in practice, could be simultaneously exploited to consistently extract a precise value for Γ_t.

Since there are two decaying top quarks, the method applied for the Higgs boson (discussed in section 1.1) has to be extended to consider the various resonance regions formed by both the top and antitop invariant masses. Given top quarks decay to W-bosons and b-quarks (measured as b-flavoured jets J_b and $J_{\bar{b}}$ in experiments), the invariant masses one has to consider are those of *reconstructed* top quarks, namely $M(W^+, J_b)$ and $M(W^-, J_{\bar{b}})$. We first try to provide some insight into the structure of the $W^+W^-b\bar{b}$ cross section by considering different resonance regions of the reconstructed masses, $M(W^+, J_b)$ and $M(W^-, J_{\bar{b}})$. The cross section can be divided up into double, single and non-resonant contributions, where these configurations can be quantified according to the value of the measured invariant masses as follows:

$$
\begin{aligned}
\text{double resonant:} \quad & M(W^+, J_b) \sim m_t^2 \ \text{ and } \ M(W^-, J_{\bar{b}}) \sim m_t^2 \\
\text{single resonant:} \quad & M(W^+, J_b) \sim m_t^2 \ \text{ and } \ \left\{ M(W^-, J_{\bar{b}}) \ll m_t^2 \ \text{ or } \ M(W^-, J_{\bar{b}}) \gg m_t^2 \right\} \\
\text{single resonant:} \quad & \left\{ M(W^+, J_b) \ll m_t^2 \ \text{ or } \ M(W^+, J_b) \gg m_t^2 \right\} \ \text{ and } \ M(W^-, J_{\bar{b}}) \sim m_t^2 \\
\text{non resonant:} \quad & \left\{ M(W^+, J_b) \ll m_t^2 \ \text{ or } \ M(W^+, J_b) \gg m_t^2 \right\} \ \text{ and } \\
& \left\{ M(W^-, J_{\bar{b}}) \ll m_t^2 \ \text{ or } \ M(W^-, J_{\bar{b}}) \gg m_t^2 \right\}.
\end{aligned}
\tag{3.1}
$$

We note that the way in which we have chosen to define the different resonance regions depends on being able to faithfully tag a b-jet and a $\bar{b}$-jet.[4] Although challenging, discriminating between bottom quark and antiquark jets does appear to be possible at a Linear Collider, see for example the discussion in ref. [81] which proposes a novel quark-charge reconstruction algorithm to allow for such a selection. Since we consider the process with onshell W-bosons, we have also made the assumption of perfectly reconstructed W-bosons. These are clearly theoretical idealisations, but they nevertheless allow us to explore effects and features that would be present in a setup that additionally includes detailed simulations of other experimental effects (combinatorics, detector effects, etc).

The full matrix element comprising of the complete set of diagrams has a non-trivial dependence on several couplings. However, the coupling structure of the amplitudes giving the dominant contributions in the different resonant regions can be simplified. In the double resonant region, as defined in eq. (3.1), the leading contributions are given by the

[4] The precise way in which one divides up the phase space is of course arbitrary (see discussion later).

double-resonant diagrams, and in this region the matrix element squared can be written as

$$\left|\mathcal{M}^{\mathrm{DR}}\right|^2 = \Big|\sum_{V\in\{\gamma,Z\}} g_{eeV}\, g_{ttV}\, A_V^{\mathrm{DR}}\Big|^2 \frac{g_{tbW}^4}{(m_t\Gamma_t)^2} + \text{ subleading terms}\,, \tag{3.2}$$

with A_V^{DR} denoting the amplitude for $e^+e^- \xrightarrow{V} t\bar{t} \to W^+W^-b\bar{b}$ (see figure 1(a)).[5] In the above equation we have factored out the dependence of the amplitudes on g_{tbW} as well as the denominators of the top-quark propagators which lead to the explicit factors of Γ_t.[6]

In each of the single-resonant regions defined in eq. (3.1), the leading contributions arise from a linear combination of double and single resonant amplitudes and the matrix element squared in these regions can be written schematically as

$$\left|\mathcal{M}^{\mathrm{SR}}\right|^2 = \Big|\sum_{V\in\{\gamma,Z\}} g_{eeV}\, g_{ttV}\, A_V^{\mathrm{DR}} + \sum_{V\in\{\gamma,Z\}}\sum_{j\in\{b,W\}} g_{eeV}\, g_{jjV}\, A_{Vj}^{\mathrm{SR}} + g_{eeW}^2\, A_W^{\mathrm{SR}}\Big|^2 \frac{g_{tbW}^4}{m_t\Gamma_t}$$
$$+ \text{ subleading terms}\,. \tag{3.3}$$

A_{Vj}^{SR} and A_W^{SR} are amplitudes arising from diagrams with a single resonant top quark, such as those in figure 1(b) and (c) respectively. The structure above can be understood as comprising of the single resonant component of the double resonant amplitudes (see figure 1(a)) and contributions from the single resonant amplitudes themselves (see figure 1(b) and (c)). Given that only one reconstructed top is resonant, the matrix element scales as Γ_t^{-1}, however, interestingly, these contributions scale with the same power of g_{tbW} as for the double resonant case.

We now consider the ratio of the single resonant and double resonant region, which, following previous arguments is insensitive to explicit powers of the coupling g_{tbW}. However, this ratio is (up to subleading terms) linearly dependent on the width,

$$\frac{\sigma^{\text{single-resonant}}}{\sigma^{\text{double-resonant}}} \propto \Gamma_t\,. \tag{3.4}$$

This means that the ratio we consider above indeed is a probe of Γ_t and is largely independent of variations in g_{tbW}. Of course, Γ_t is itself sensitive to departures of g_{tbW} from the SM value, but may also change without modifications to the g_{tbW} coupling and the latter possibility is one we wish to allow for. The statement of eq. (3.4) holds at leading order and as we will see requires some refining when taking into account higher orders. It is also dependent on the assumption that all couplings involved in the process take their SM values. Should the couplings g_{ttV} differ from their SM values, the ratio of single- and double-resonant contributions will in general be altered and the determination of the top-quark width becomes more involved. We note that subsequently when varying the top-quark width Γ_t we hold the coupling g_{tbW} fixed at its SM value. A priori, a common rescaling of $g_{tbW} \to \xi g_{tbW}$ and $\Gamma_t \to \xi^2\Gamma_t$ leaves the double resonant squared matrix element invariant, whereas the single resonant region is rescaled. Therefore, eq. (3.4) provides

[5] The couplings g_{ijk} arise from the Feynman rules for the vertices involving the particles i, j and k.

[6] Note we have used the standard expansion $\frac{1}{(p_X-m_X)^2+m_X^2\Gamma_X^2} \to \frac{\pi}{m_X\Gamma_X}\delta(p_X^2-m_X^2) + \mathcal{O}\left(\frac{\Gamma_X}{m_X}\right)$ which holds in the limit $p_X^2 \to m_X^2$ applied at the matrix element squared level.

the relevant counterpart ratio in the process $e^+e^- \to W^+W^-b\bar{b}$ that corresponds to the ratio taken in studies for the Higgs boson width.

The sets of amplitudes we have isolated in eqs. (3.2) and (3.3) are not themselves gauge-invariant; gauge invariance is restored once all subleading terms are included, which of course is the case for the full amplitudes we actually work with. However, it is nevertheless true that the amplitudes written down in these equations give the leading contributions in the double and single resonant regions. We note that approaches such as the pole expansion [82, 83] or an effective theory expansion [80, 84, 85] provide gauge-invariant methods to compute cross sections to higher order in the different resonance regions without having to consider the full final-state amplitude. In such expansions the dominant terms in double and single resonant regions indeed receive their contributions from eqs. (3.2) and (3.3). This therefore argues strongly in favour of the scaling of the ratio in eq. (3.4) as well as for it being virtually independent of g_{tbW}.

3.1 Dividing up the cross section

In the previous subsection we argued that the ratio of single resonant to double resonant cross sections may provide a handle on the top-quark width. Here we set up a feasibility study of such a measurement, discussing in particular the care required in choosing the resonance regions.

According to the discussion above and in particular eq. (3.1) the cross section for $e^+e^- \to W^+W^-b\bar{b}$ can be divided up into double, single and non-resonant regions in the double differential distribution $d^2\sigma/dM(W^+, J_b)dM(W^-, J_{\bar{b}})$. We define reconstructed top and antitop quarks to be resonant if $M(W^+, J_b) \in [M_{\min}, M_{\max}]$ GeV and $M(W^-, J_{\bar{b}}) \in [M_{\min}, M_{\max}]$ GeV respectively. The cross section resonance regions can then be categorized as

$$\begin{aligned}
&\text{double resonant (DR):} && M(W^+, J_b) \in [M_{\min}, M_{\max}] \text{ and } M(W^-, J_{\bar{b}}) \in [M_{\min}, M_{\max}] \\
&\text{single resonant 1 (SR1):} && M(W^+, J_b) \in [M_{\min}, M_{\max}] \text{ and } M(W^-, J_{\bar{b}}) > M_{\max} \\
&&& \text{or } M(W^+, J_b) > M_{\max} \text{ and } M(W^-, J_{\bar{b}}) \in [M_{\min}, M_{\max}] \\
&\text{single resonant 2 (SR2):} && M(W^+, J_b) \in [M_{\min}, M_{\max}] \text{ and } M(W^-, J_{\bar{b}}) < M_{\min} \\
&&& \text{or } M(W^+, J_b) < M_{\min} \text{ and } M(W^-, J_{\bar{b}}) \in [M_{\min}, M_{\max}] \,. \qquad (3.5)
\end{aligned}$$

We use the notation σ^{DR}, σ^{SR1}, σ^{SR2} to denote the cross section of the $W^+W^-b\bar{b}$ process in these phase space regions. We have chosen not to list the non resonant regions above. This is because for the setup we study, the cross sections for these are negligible compared to those in the DR, SR1 and SR2 regions and therefore we do not consider them useful in this context. The boundaries $\big(M_{\min}, M_{\max}\big)$ determine the size of the resonant region for each reconstructed top quark. The exact values are of course arbitrary and we vary them in three sets $\big(M_{\min}, M_{\max}\big) \in \big\{(165, 180), (160, 185), (155, 190)\big\}$ GeV.[7]

[7] We note that $\big(M_{\min}, M_{\max}\big) = (165, 180)$ GeV (roughly) represent the boundaries outside which the effects of Γ_t in the Breit-Wigner propagator are smaller than 1 %, i.e. for $M > 160$ GeV or $M > 185$GeV, we have that $((p_t^2 - m_t^2)^2 + m_t^2\Gamma_t^2)/(p_t^2 - m_t^2)^2 < 1.01$.

The reason for having two separate single resonant (SR1 and SR2) regions has to do with higher-order corrections to the cross section. As we explained in section 2.3 and is clearly visible in figure 4, in the region of $M(W^+, J_b), M(W^-, J_{\bar{b}}) < M_{\text{min}}$ the cross section is highly sensitive to additional gluon radiation from the decay products of a resonant intermediate top quark. This means that the SR2 region will tend to receive very large NLO corrections from double resonant real contributions in which gluon emissions are not captured in the appropriate b or $\bar{b}$ jet. As such the SR2 region is likely to suffer from a significantly larger renormalization scale dependence than the SR1 region. It is therefore, in practice, much less sensitive to variations in the top-quark width than a LO analysis may naively find. Since the size of this effect is dependent on the choice made for R_{jet} we investigate the impact of varying the jet radius has on the final results.

We study the impact on the structure of the cross section when varying the SM top-quark width by $\pm 20\%$ and fixing the coupling g_{tbW}. The LO cross section is independent of μ_R since the tree-level diagrams do not depend on α_s. The NLO cross section does however depend on the renormalization scales and this dependence must be quantified if a reliable estimate of the sensitivity to Γ_t is to be made.

In figure 7(a) we plot the dependence on μ_R of the fiducial cross section (thick solid blue), as well as the μ_R-dependence of its double and resonant sub-regions: DR (thin solid blue), SR1 (long dashed blue) and SR2 (dotted blue). As also seen in figure 2, the total fiducial cross section is only very mildly dependent on μ_R. However, figure 7(a) reveals that both DR and SR2 cross sections carry a dependence on μ_R and, moreover, that their dependence goes in opposite directions. This crucially means that the ratio SR2/DR has a large dependence on μ_R, thus making it essentially insensitive within uncertainties to the relatively small variations in Γ_t we consider. On the other hand, the SR1 region is largely independent on μ_R, making the ratio SR1/DR a potentially good one for probing Γ_t. These patterns will be confirmed in the figures that follow. We note that similar conclusions as for the SR2 region hold for the total single resonant region SR1+SR2 since the latter is dominated in size and in scale-dependence by the SR2 region (see the short dashed gray curve in figure 7(a)). For this reason we do not consider the full single resonant region any further.

Figure 7(b) shows the Γ_t-dependence of the DR, SR1 and SR2 regions at LO (green) and NLO (blue). The clear $1/\Gamma_t^2$ behaviour of the double resonant region both at LO and NLO illustrates that while varying the top-quark width we hold g_{tbW} fixed. This also illustrates our earlier arguments that the NLO corrections to the SR2-region cross section are indeed very large, whilst the corrections to SR1 show a better behaviour. Whilst the actual size of NLO corrections in each region is dependent on R_{jet}, these observations are generically true over all values of R_{jet} that we have considered (i.e. $R_{\text{jet}} \in [0.5, 1.3]$). As also anticipated the σ^{SR2} contribution shows a sizeable dependence on μ_R, whilst σ^{SR1} appears relatively unaffected by the variation.

With an understanding of the structure of NLO corrections as well as the scale dependence of the various resonance regions we can now move to studying the ratios of interest.

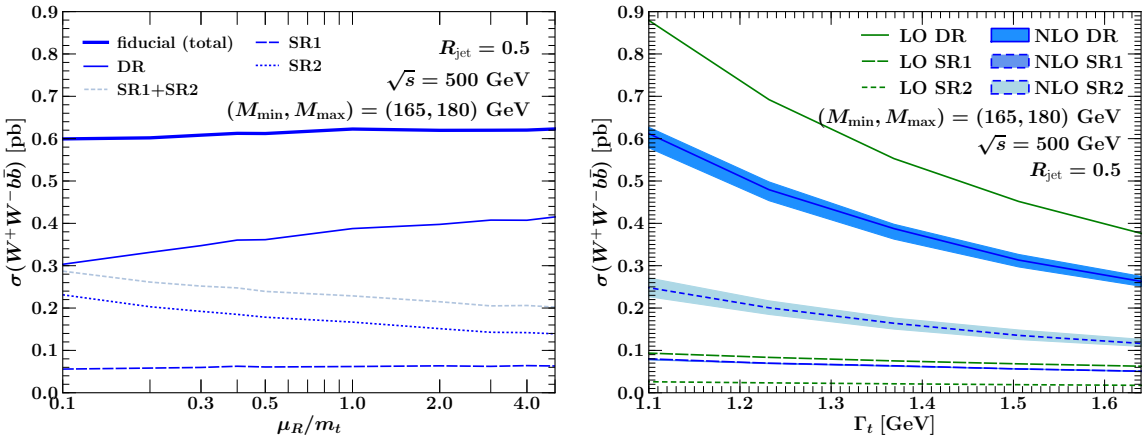

Figure 7. (a) Dependence on the renormalization scale of the NLO cross sections in the double and single resonant regions as defined in eq. (3.5). (b) Dependence of LO and NLO DR, SR1 and SR2 cross sections on the top-quark width. The plots above illustrate the results for the choice $R_{\rm jet} = 0.5$ and $M_{\rm min} = 165$ GeV and $M_{\rm min} = 180$ GeV.

Specifically we examine the cross section ratios:

$$\frac{\sigma^{\rm SR1}}{\sigma^{\rm DR}} \quad \text{and} \quad \frac{\sigma^{\rm SR2}}{\sigma^{\rm DR}} \,. \tag{3.6}$$

In order to verify the independence of our ratios on the coupling g_{tbW}, we have checked numerically that varying g_{tbW} by $\pm 10\%$ while keeping Γ_t fixed, indeed leaves the ratios unchanged.

In each of the plots in figure 8 the ratios $\sigma^{\rm SR1}/\sigma^{\rm DR}$ (long dashes) and $\sigma^{\rm SR2}/\sigma^{\rm DR}$ (short dashes) are shown. LO and NLO results are in green and blue respectively and the bands around the NLO results indicate the uncertainty due to μ_R-variation. From left-to-right in figure 8 the jet radius parameter is varied, $R_{\rm jet} \in \{0.5, 1.3\}$, i.e. going left-to-right illustrates the effect of increasing the size of the jet-radius. From top-to-bottom in figure 8 we have varied the definition of the resonance region – specifically a reconstructed top is defined to be resonant if $M(W^+, J_b) \in \{(165, 180),\ (160, 185),\ (155, 190)\}$ GeV, i.e. going top-to-bottom the resonance region is widened.

In general, it is observed that at LO and NLO both ratios $\sigma^{\rm SR1}/\sigma^{\rm DR}$ and $\sigma^{\rm SR2}/\sigma^{\rm DR}$ display a roughly linear dependence on Γ_t, as might be expected from the naive counting arguments given in the discussion preceding eq. (3.4). For the latter ratio however the dependence is actually much flatter, whereas the former ratio importantly shows a stronger dependence on the top-quark width (i.e. the gradient is steeper).

For $R_{\rm jet} = 0.5$ at NLO, see plots (a), (c) and (e) of figure 8, the ratio $\sigma^{\rm SR2}/\sigma^{\rm DR}$ suffers from a large μ_R-variation uncertainty (of real emission origin as discussed previously). In contrast and as expected, $\sigma^{\rm SR1}/\sigma^{\rm DR}$ only has a small corresponding uncertainty for $R_{\rm jet} = 0.5$. Widening the jet radius leads to the scale uncertainty increasing for $\sigma^{\rm SR1}/\sigma^{\rm DR}$ and decreasing for $\sigma^{\rm SR2}/\sigma^{\rm DR}$. For the results with $R_{\rm jet} = 1.3$ displayed in plots (b), (d) and (f) of figure 8, we see that the uncertainty bands of the two ratios have roughly the

same thickness. As explained in section 2.3, the reason for this is that a larger jet radius means that less radiation is leaked out of the b-jet for emissions from the top decay whilst unfortunately allows more radiation into the b-jet when emissions come from elsewhere in the $W^+W^-b\bar{b}$ process. These two effects combine to increase the size of NLO corrections and scale dependence of $M(W^+, J_b) < m_t$ and have the opposite effect for $M(W^+, J_b) > m_t$, as we also saw in figure 4. The same reason lies behind the observed pattern that with increasing jet radius the ratios $\sigma^{\rm SR1}/\sigma^{\rm DR}$ and $\sigma^{\rm SR2}/\sigma^{\rm DR}$ are enhanced and diminished respectively. By minimising non-top-resonance-decay radiation ending up in the b-jets, it is highly plausible that the use of modern jet-substructure techniques may help to control the behaviour of the SR1 region for increasing $R_{\rm jet}$.

As stressed above, precisely where one chooses to split the cross section into its various resonance regions is a little arbitrary and variations of this choice should be studied. In figure 8 going from top-to-bottom the ratios of cross sections decrease in size, however the pattern for the ratios of cross sections remains the same. This is due to the fact that by widening the definition of the resonances one naturally reduces the single resonant regions while at the same time increasing the double resonant one. The patterns remain the same because we have chosen to widen the resonance window in a symmetric manner. Of course, one is free to pick different (e.g. asymmetric) resonance regions, however the patterns and results we present here are unlikely to change dramatically.

Overall the ratio $\sigma^{\rm SR1}/\sigma^{\rm DR}$ exploiting the region $M(W^+, J_b) > m_t$ appears as the more useful of the two to probe Γ_t. The large scale dependence together with the flatness of the ratio $\sigma^{\rm SR2}/\sigma^{\rm DR}$ make this ratio rather unsuitable for a width-extraction.[8] To quantify the potential sensitivity this approach may achieve and to compare the different setups, we provide possible accuracies on Γ_t in two scenarios. Firstly, we assume a measurement of the ratio of $\sigma^{\rm SR1}/\sigma^{\rm DR}$ with infinite experimental precision, which due to our theoretical (scale) uncertainty translates into an uncertainty $\Delta\Gamma_t^{\rm theo}$. Secondly, we assume a fixed experimental error on the ratio $\sigma^{\rm SR1}/\sigma^{\rm DR}$ of ± 0.005, which corresponds to a measured accuracy of the ratio of $5-10\%$. This enlarges the uncertainty of $\Delta\Gamma_t^{\rm theo}$ to $\Delta\Gamma_t$ as shown in table 2. The table also depicts the setups presented in section 3.2. We conclude that better sensitivities are obtained for a small jet radius $R_{\rm jet}$ in case of an unpolarised initial state and $\sqrt{s} = 500\,\text{GeV}$. We also observe that while increasing the interval $(M_{\rm min}, M_{\rm max})$ generally improves the sensitivity $\Delta\Gamma_t^{\rm theo}$, the actual number of events is diminished in the single resonant region leading to a smaller value for the ratio $\sigma^{\rm SR1}/\sigma^{\rm DR}$. When assuming an absolute error on the measurement of the ratio, this smaller value results in larger uncertainties $\Delta\Gamma_t$.

We have checked that for $\sqrt{s} = 500\,\text{GeV}$ and an integrated luminosity of $500\,\text{fb}^{-1}$ several thousands of events can be recorded, even in the single resonant region SR1. The difficulties of the method are thus not in collecting enough statistics, but in a proper reconstruction of the invariant mass.

[8] Exactly the same conclusions hold for a ratio involving the total single resonant region, namely $(\sigma^{\rm SR1} + \sigma^{\rm SR2})/\sigma^{\rm DR}$.

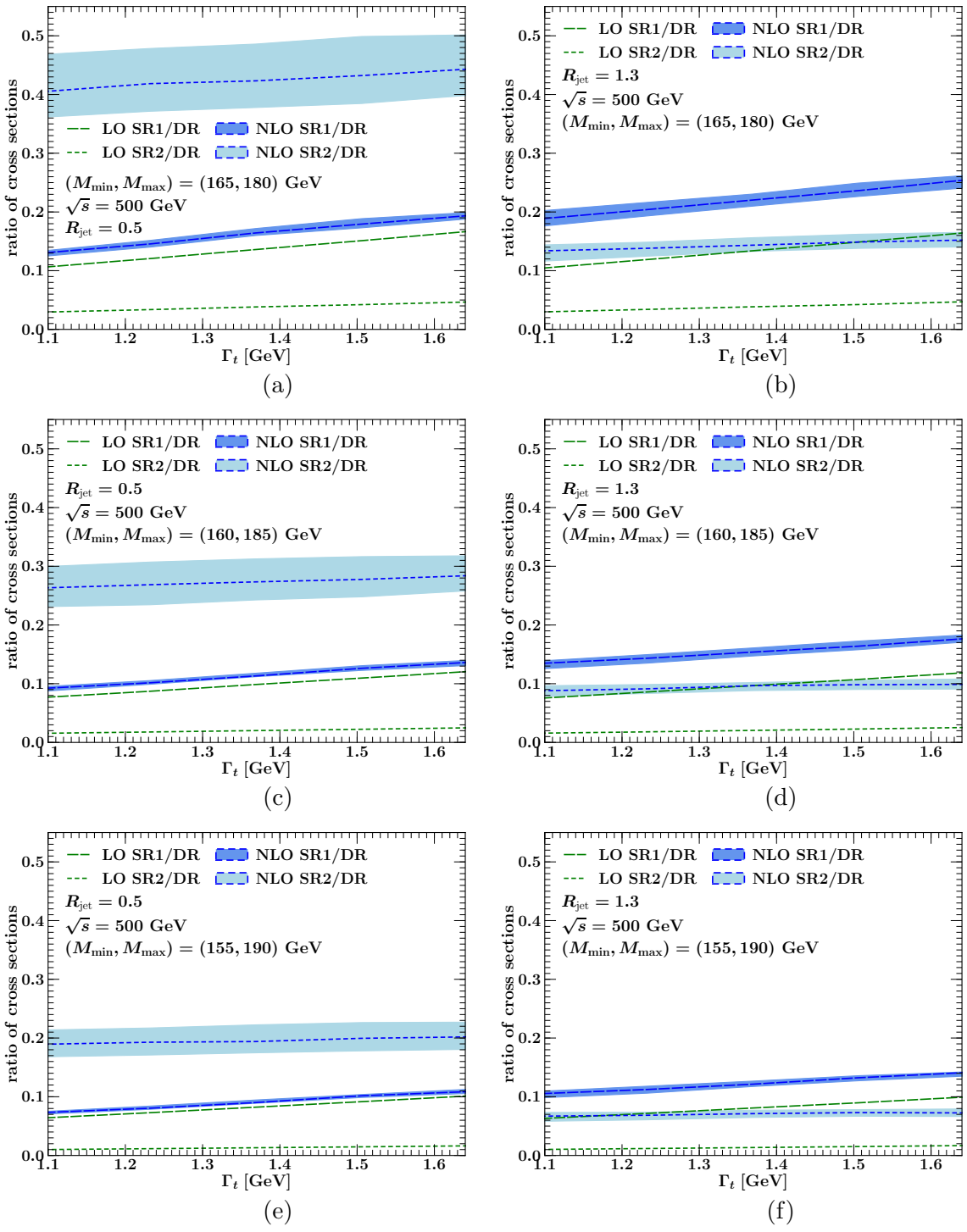

Figure 8. Dependence on Γ_t of the ratios of the single resonant cross sections, SR1 (long dashed curves) and SR2 (short dashed curves) to the double resonant, DR, cross section, see eq. (3.5) for definitions. Ratios of LO and NLO cross sections are shown in green and blue respectively and bands are obtained via variation of μ_R. The left-hand plots (a,c,e) show the results for $R_{\rm jet} = 0.5$ whilst the right-hand plots (b,d,f) illustrate the results for $R_{\rm jet} = 1.3$. Plots (a,b), (c,d) and (e,f) illustrate the ratios for $(M_{\rm min}, M_{\rm max}) = (165, 180)$ GeV, $(160, 185)$ GeV and $(155, 190)$ GeV respectively. All results are for $\sqrt{s} = 500$ GeV.

$\sqrt{s}$ [GeV]	Pol.	R_{jet}	$(M_{\text{min}}, M_{\text{max}})$ [GeV]	$\Delta\Gamma_t^{\text{theo}}$ [GeV]	$\Delta\Gamma_t$ [GeV]
500	unpol.	0.5	(165, 180)	0.11	0.19
500	unpol.	1.3	(165, 180)	0.19	0.27
500	unpol.	0.5	(160, 185)	0.10	0.20
500	unpol.	1.3	(160, 185)	0.19	0.31
500	unpol.	0.5	(155, 190)	0.09	0.25
500	unpol.	1.3	(155, 190)	0.20	0.36
500	$(-1, +1)$	0.5	(165, 180)	0.07	0.14
600	unpol.	0.5	(165, 180)	0.12	0.18

Table 2. Sensitivities on the top-quark width for different setups of the centre-of-mass energy $\sqrt{s}$, the polarisation, given as (P_{e^+}, P_{e^-}), the jet radius R_{jet} and the interval $(M_{\text{min}}, M_{\text{max}})$.

3.2 Improved width extractions

There are a number of ways to exploit possible linear collider setups to improve the sensitivity of the method explored in the previous section on the top-quark width. The two ways we consider here are using polarised beams and increasing the centre of mass energy, both of which tend to enhance the proportion of single resonant to double resonant contributions to the $W^+W^-b\bar{b}$ cross section.

3.2.1 Exploiting polarised beams

So far, our discussion has been based on simulations where the helicities of the incoming electron and positron were averaged over. However, a powerful feature of a linear collider is the fact that the initial state electron and positron beams can be polarised. Given the electroweak nature of the primary interactions of the processes under consideration, the inclusive cross section σ can be decomposed according to [86]

$$\sigma = \frac{1}{4}\,(1 - P_{e^+})\,(1 + P_{e^-})\,\sigma_{-1+1} + \frac{1}{4}\,(1 + P_{e^+})\,(1 - P_{e^-})\,\sigma_{+1-1}\,, \tag{3.7}$$

where P_{e^+} and P_{e^-} denote the relative polarisation of the positron and electron beam respectively. σ_{xy} encodes the cross section obtained with fixed helicities x for the positron e^+ and y for the electron e^-. Whereas the double resonant diagrams contribute to both parts σ_{-1+1} and σ_{+1-1} several single resonant and non resonant diagrams only contribute to the combination σ_{+1-1}. Therefore, the single resonant contributions can be enhanced by choosing the $(P_{e^+}, P_{e^-}) = (+1, -1)$ combination. We note that eq. (3.7) is also valid at the level of differential cross sections, i.e. we can replace all occurrences of the inclusive cross section σ with e.g. $d\sigma/dM(W^+, J_b)$ at LO and NLO in QCD. We obtained polarised initial states in MadGraph5_aMC@NLO by adapting the model files such as to select only left- or right-handed couplings appropriately. We have validated our results at LO through a comparison to results with explicit polarisations (available in the LO version of the MadGraph5_aMC@NLO code) and at NLO by ensuring that we could reproduce the unpolarised cross section using eq. (3.7).

In figure 9(a) we show the differential cross section as a function of $M(W^+, J_b)$ for the unpolarised initial state as discussed beforehand, but also for two common polarisa-

tions $(P_{e^+}, P_{e^-}) = (0.3, -0.8)$ and $(P_{e^+}, P_{e^-}) = (-0.3, +0.8)$ at a linear collider.[9] We find that the inclusive cross section increases the closer the polarisation is to σ_{+1-1}, i.e. $(P_{e^+}, P_{e^-}) = (+1, -1)$. This increase is even more pronounced for the single resonant part of the cross section, as is apparent in figure 9(b). In the latter figure we show the ratio of the combination σ_{-1+1} over the combination σ_{+1-1}, both at LO and NLO QCD. Whereas at LO the rise for low values of $M(W^+, J_b)$ is dramatic due to the vanishing of single and non resonant diagrams for σ_{-1+1}, the ratio at NLO QCD remains rather constant in the region $M(W^+, J_b) \leq m_t$. Again this effect is induced by the real emission of gluons from double resonant diagrams. As expected LO and NLO ratios are much closer in the single resonant region SR1 with $M(W^+, J_b) > m_t$.

Taking all of this into account, it is evident that the sensitivity to the top-quark width can thus be significantly increased by the combination $(P_{e^+}, P_{e^-}) = (-1, +1)$. For this particular case we show the corresponding sensitivity in figure 10 obtained for a jet radius of $R_{\text{jet}} = 0.5$. Compared to the unpolarised case (figure 8(a)) we see that not only is the ratio $\sigma^{\text{SR1}}/\sigma^{\text{DR}}$ increased in size, but also its gradient is visibly enhanced (by about 23 % for the setup considered). We perform the study of extracting Γ_t in the two scenarios described at the end of section 3.1 and indicate the corresponding accuracies in table 2, which we find to be significantly improved compared to the unpolarised case.

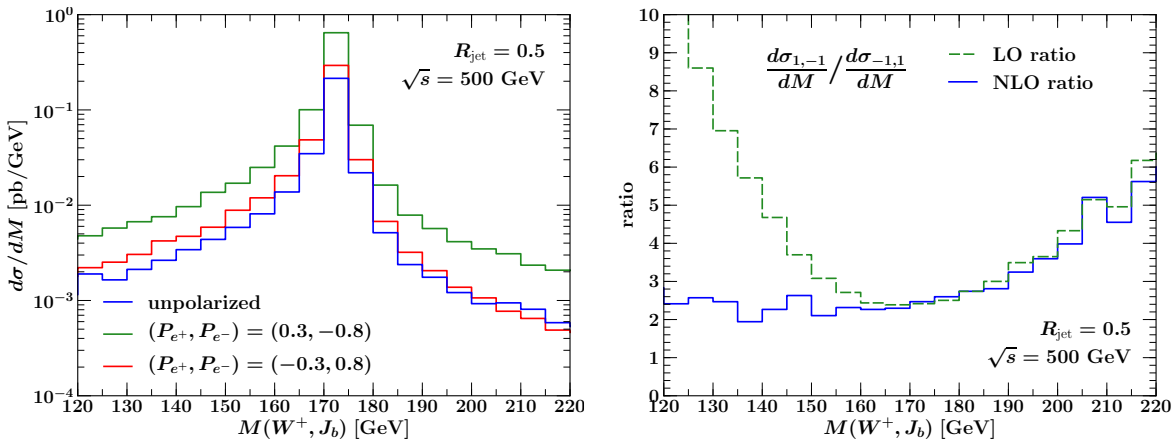

Figure 9. (a) NLO cross section as a function of $M(W^+, J_b)$ in GeV for different polarisations of the initial electron and positron: unpolarised (blue), $(P_{e^+}, P_{e^-}) = (0.3, -0.8)$ (green) and $(P_{e^+}, P_{e^-}) = (-0.3, +0.8)$ (red); (b) Ratio of cross sections with $(P_{e^+}, P_{e^-}) = (1, -1)$ over $(P_{e^+}, P_{e^-}) = (-1, 1)$ at LO (dashed green) and NLO (black) as a function of $M(W^+, J_b)$ in GeV. All results are for $\sqrt{s} = 500$ GeV and $R_{\text{jet}} = 0.5$. We note that the results for $R_{\text{jet}} = 1.3$ (not shown) are similar.

3.2.2 Exploiting a higher centre of mass energy

Due to the increase by more than a factor of 4 of the cross section of $e^+e^- \to t\bar{t}H$ (relevant for the measurement of the top-Yukawa coupling) when going from a centre of mass energy

[9] The chosen polarisation degrees are those foreseen for the current baseline design, however, higher polarisation degrees for both beams could be achieved at a later stage.

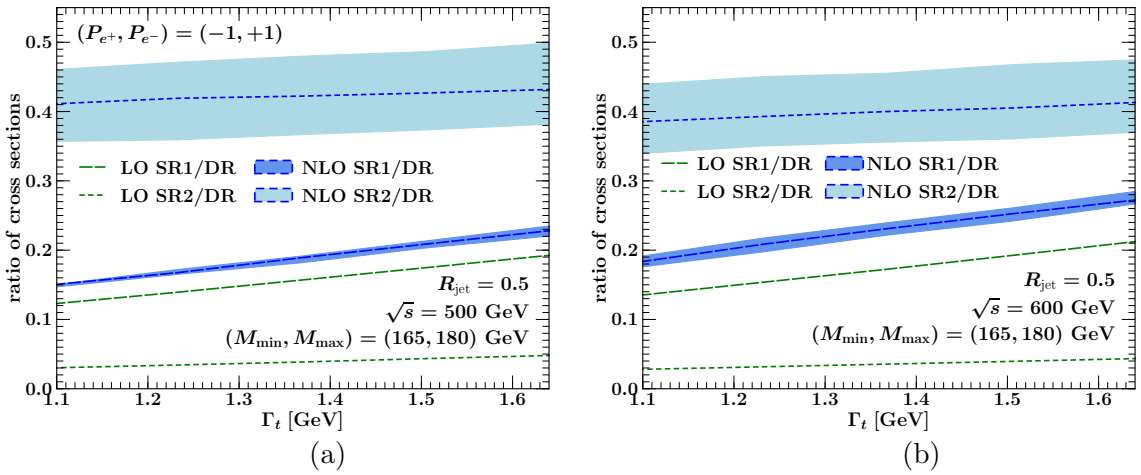

Figure 10. Dependence on Γ_t of the ratios of the single resonant cross sections, SR1 (long dashed curves) and SR2 (short dashed curves) to the double resonant, DR, cross section, see eq. (3.5) for definitions. Ratios of LO and NLO cross sections are shown in green and blue respectively and bands are obtained via variation of μ_R. Plot (a) shows the results for polarised beams $(P_{e^+}, P_{e^-}) = (-1, +1)$ at $\sqrt{s} = 500$ GeV, whilst plot (b) shows the patterns for unpolarised beams for a higher centre of mass energy of $\sqrt{s} = 600$ GeV. All results are for $R_{\text{jet}} = 0.5$.

of 500 GeV to 600 GeV, a slightly higher initial centre of mass energy at a linear collider is well-motivated. Hence, in this subsection we present the sensitivity on the top-quark width for $\sqrt{s} = 600$ GeV. Once again we study the ratios of eq. (3.6), showing these in figure 10(b), and again using $R_{\text{jet}} = 0.5$. We again find that not only is the relevant ratio $\sigma^{\text{SR1}}/\sigma^{\text{DR}}$ increased in size, but additionally the sensitivity on the top-quark width is enhanced, with the gradient of the slope increased by about 38 % in the setup considered. Even though the scale uncertainty increases in size (thus increasing $\Delta\Gamma_t^{\text{theo}}$), the accuracy on Γ_t when an experimental error is included, $\Delta\Gamma_t$, is still slightly improved compared to the case of $\sqrt{s} = 500$ GeV due to the enhancement of the gradient. The relevant numbers on the sensitivity can be found in table 2.

3.3 Opportunities and limitations of the method

We have shown that the ratio $\sigma^{\text{SR1}}/\sigma^{\text{DR}}$ is a promising observable for extracting the top-quark width, independently from g_{tbW}, in a generic analysis of the $W^+W^-b\bar{b}$ process at a linear collider. An extraction of Γ_t for different choices of the resonance windows used (eq. (3.5)) not only provides an in-built consistency check on the method and measurements, but also (through the combination of these extractions) may allow for the shrinking of uncertainties in Γ_t. Furthermore, we emphasise that providing a method complementary to a lineshape fit, that additionally allows for deviations of Γ_t independently of variations in g_{tbW}, is of significant value. An interesting avenue to explore would also be to assume a fixed value for Γ_t and investigate the extent to which our method can disentangle the g_{ttV} couplings from g_{tbW} (top-pair production is sensitive to the product $g_{ttV}g_{tbW}^2$).

For the investigation we have presented in this work some assumptions have been made.

Firstly, we have assumed a perfect b and $\bar{b}$ jet-tagging as well as a perfect reconstruction of W-bosons. A more sophisticated analysis could include errors due to mistagging etc. Such uncertainties are unlikely to affect the theory results strongly and can rather be included as an experimental error. An additional assumption we have made is that the couplings appearing in the amplitudes for $e^+e^- \to W^+W^-b\bar{b}$ all take their (fixed) SM values. Clearly if couplings such as g_{ttZ} were to differ from their SM value, then the ratios predicted would also change, thus skewing the extracted width. This potential problem can be overcome by using as inputs to our method, values for the couplings as constrained in other collider processes.

The simulation underlying this work is a parton-level simulation, namely one that does not include the effects of parton-showering and hadronization. These two steps beyond a fixed-order simulation are known to alter some distribution shapes significantly. While it is therefore important to extend our results to include these effects,[10] (and thus any potential shape distortions to invariant mass distributions) we expect that, after parton-showering and hadronization, the changes to the resonance regions that arise from variations in Γ_t are very similar to those observed in our fixed-order analysis, and therefore that the ratios remain a very good probe of Γ_t. Moreover, jet-substructure techniques could be employed to understand and control radiation in an event such that the split into the resonance regions and the structure of the cross section within these is not altered significantly from the fixed-order analysis we have discussed. Therefore, we fully expect that our conclusions and the usefulness of the method to be largely unaltered.

We end this section with a few comments regarding the applicability of this method for Γ_t-extraction at the LHC from the $pp \to W^+W^-b\bar{b}$ process. This process has received significant attention recently and NLO QCD corrections to the full process are known [71–73, 75, 76]. While certainly a possibility worth exploring (one which is however beyond the scope of this work) the proton-proton initiated process intrinsically contains some difficulties. The ratio of the leading parts of the squared matrix element in the single and double resonant regions will in principle be sensitive to Γ_t, for the same arguments presented in section 3. However, given that at LO the squared matrix element is proportional to α_s^2 and that the predicted cross section additionally carries a dependence on a factorization scale, μ_F, the uncertainty due to the variation of these scales is significantly larger than that observed in this study (see discussions in the references cited above), in particular for exclusive observables. Though the ratio $\sigma^{\mathrm{SR1}}/\sigma^{\mathrm{DR}}$ may indeed be quite sensitive to Γ_t, we feel it is very likely that the uncertainty on the ratio would make an extraction prohibitive in practice (much like we have demonstrated for the ratio $\sigma^{\mathrm{SR2}}/\sigma^{\mathrm{DR}}$), even using the state-of-the-art NLO computations. It is of course possible, that with some modifications or in combination with additional measurements, such ratios would also be useful in a hadron-collider environment.

[10] This can be done within the framework of MadGraph5_aMC@NLO as well as that of the WHIZARD Event Generator, though the consistent matching to parton shower of the $W^+W^-b\bar{b}$ process is not totally straightforward and requires care due to the presence of intermediate coloured resonances (see the discussions in refs. [87, 88]).

4 Conclusions

We have performed a detailed study of the $e^+e^- \to W^+W^-b\bar{b}$ process at NLO in QCD using MadGraph5_aMC@NLO to simulate the fixed-order results. In particular we have examined the structure of reconstructed top-quark masses which has allowed for a detailed understanding of the double, single and non resonant contributions of the total cross section. We have used this to show that the ratio of single resonant to double resonant cross section contributions is sensitive to the top-quark width whilst simultaneously being independent of the g_{tbW} coupling. The central results of this article are the in-depth investigation of this ratio. We have shown in a typical linear collider analysis, that with a careful definition or choice of the single resonant region of the cross section, that such a ratio is, also in practice, sensitive to the value of Γ_t, and can be exploited to extract the width at an e^+e^- collider. We have explored the effects that variations in both the jet radius as well as in the resonance window (in which reconstructed top quarks are defined to be resonant) have on the ratios. Additionally, we showed that using polarised beams or higher centre of mass energies leads to an enhanced sensitivity to Γ_t. In a study of the expected errors in the extraction of Γ_t using this method, we find that attainable accuracies of < 200 MeV are possible with unpolarised beams at $\sqrt{s} = 500$ GeV. We note that these are comparable to the accuracies quoted in the literature obtained from invariant-mass lineshape fitting, and that they can be significantly improved by exploiting polarised initial states.

Our study of the $e^+e^- \to W^+W^-b\bar{b}$ process here has been restricted to fixed-order. The next step in extending this investigation is to include effects due to parton-showering and hadronization, which we look forward to investigating in future work.

5 Acknowledgements

This work has received the support of the Collaborative Research Center SFB676 of the DFG, "Particles, Strings, and the Early Universe." The work of AP is supported by the UK Science and Technology Facilities Council [grant ST/L002760/1].

References

[1] **ATLAS** Collaboration, G. Aad et al., *Observation of a new particle in the search for the Standard Model Higgs boson with the ATLAS detector at the LHC*, *Phys. Lett.* **B716** (2013) 1–29, [arXiv:1207.7214].

[2] **CMS** Collaboration, S. Chatrchyan et al., *Observation of a new boson at a mass of 125 GeV with the CMS experiment at the LHC*, *Phys. Lett.* **B716** (2013) 30–61, [arXiv:1207.7235].

[3] T. Behnke et al., *The International Linear Collider Technical Design Report - Volume 1: Executive Summary*, arXiv:1306.6327.

[4] H. Baer et al., *The International Linear Collider Technical Design Report - Volume 2: Physics*, arXiv:1306.6352.

[5] C. Adolphsen et al., *The International Linear Collider Technical Design Report - Volume 3.I: Accelerator & in the Technical Design Phase*, arXiv:1306.6353.

[6] C. Adolphsen et al., *The International Linear Collider Technical Design Report - Volume 3.II: Accelerator Baseline Design*, arXiv:1306.6328.

[7] H. Abramowicz et al., *The International Linear Collider Technical Design Report - Volume 4: Detectors*, arXiv:1306.6329.

[8] G. Moortgat-Pick et al., *Physics at the e^+e^- Linear Collider*, *Eur.Phys.J.* (2015) [arXiv:1504.01726].

[9] K. Fujii et al., *Physics Case for the International Linear Collider*, arXiv:1506.05992.

[10] A. Juste et al., *Report of the 2005 Snowmass top/QCD working group*, *ECONF* **C0508141** (2005) PLEN0043, [hep-ph/0601112].

[11] **Top Quark Working Group** Collaboration, K. Agashe et al., *Working Group Report: Top Quark*, in *Community Summer Study 2013: Snowmass on the Mississippi (CSS2013) Minneapolis, MN, USA, July 29-August 6, 2013*, 2013. arXiv:1311.2028.

[12] T. Barklow, J. Brau, K. Fujii, J. Gao, J. List, N. Walker, and K. Yokoya, *ILC Operating Scenarios*, arXiv:1506.07830.

[13] K. G. Chetyrkin, J. H. Kühn, and M. Steinhauser, *Heavy quark current correlators to $O(\alpha_s^2)$*, *Nucl. Phys.* **B505** (1997) 40–64, [hep-ph/9705254].

[14] A. H. Hoang and T. Teubner, *Analytic calculation of two loop corrections to heavy quark pair production vertices induced by light quarks*, *Nucl. Phys.* **B519** (1998) 285–328, [hep-ph/9707496].

[15] R. Harlander and M. Steinhauser, *$O(\alpha_s^2)$ corrections to top quark production at e^+e^- colliders*, *Eur. Phys. J.* **C2** (1998) 151–158, [hep-ph/9710413].

[16] K. G. Chetyrkin, A. H. Hoang, J. H. Kühn, M. Steinhauser, and T. Teubner, *Massive quark production in electron positron annihilation to order α_s^2*, *Eur. Phys. J.* **C2** (1998) 137–150, [hep-ph/9711327].

[17] K. G. Chetyrkin, R. V. Harlander, and J. H. Kühn, *Quartic mass corrections to R(had) at order α_s^3*, *Nucl. Phys.* **B586** (2000) 56–72, [hep-ph/0005139]. [Erratum: Nucl. Phys.B634,413(2002)].

[18] W. Bernreuther, R. Bonciani, T. Gehrmann, R. Heinesch, T. Leineweber, P. Mastrolia, and E. Remiddi, *Two-loop QCD corrections to the heavy quark form-factors: The Vector contributions*, *Nucl. Phys.* **B706** (2005) 245–324, [hep-ph/0406046].

[19] W. Bernreuther, R. Bonciani, T. Gehrmann, R. Heinesch, T. Leineweber, P. Mastrolia, and E. Remiddi, *Two-loop QCD corrections to the heavy quark form-factors: Axial vector contributions*, *Nucl. Phys.* **B712** (2005) 229–286, [hep-ph/0412259].

[20] W. Bernreuther, R. Bonciani, T. Gehrmann, R. Heinesch, T. Leineweber, and E. Remiddi, *Two-loop QCD corrections to the heavy quark form-factors: Anomaly contributions*, *Nucl. Phys.* **B723** (2005) 91–116, [hep-ph/0504190].

[21] J. Gluza, A. Mitov, S. Moch, and T. Riemann, *The QCD form factor of heavy quarks at NNLO*, *JHEP* **07** (2009) 001, [arXiv:0905.1137].

[22] J. Gao and H. X. Zhu, *Electroweak prodution of top-quark pairs in e^+e^- annihilation at NNLO in QCD: the vector contributions*, *Phys. Rev.* **D90** (2014), no. 11 114022, [arXiv:1408.5150].

[23] J. Gao and H. X. Zhu, *Top Quark Forward-Backward Asymmetry in e^+e^- Annihilation at Next-to-Next-to-Leading Order in QCD*, *Phys. Rev. Lett.* **113** (2014), no. 26 262001, [arXiv:1410.3165].

[24] C. R. Schmidt, *Top quark production and decay at next-to-leading order in e^+e^- annihilation*, *Phys. Rev.* **D54** (1996) 3250–3265, [hep-ph/9504434].

[25] L. Guo, W.-G. Ma, R.-Y. Zhang, and S.-M. Wang, *One-loop QCD corrections to the $e^+e^- \to W^+W^-b\bar{b}$ process at the ILC*, *Phys.Lett.* **B662** (2008) 150–157, [arXiv:0802.4124].

[26] O. Mattelaer, *MadGraph5_AMC@NLO and top pair production at a Linear Collider*, *Nuovo Cim.* **C037** (2014), no. 02 61–67.

[27] C. Weiss, B. C. Nejad, W. Kilian, and J. Reuter, *Automated NLO QCD Corrections with WHIZARD*, in *PoS(EPS-HEP2015)466, 2015*, 2015. arXiv:1510.02666.

[28] S. Dittmaier and M. Roth, *LUSIFER: A LUcid approach to six FERmion production*, *Nucl. Phys.* **B642** (2002) 307–343, [hep-ph/0206070].

[29] S. Fleming, A. H. Hoang, S. Mantry, and I. W. Stewart, *Jets from massive unstable particles: Top-mass determination*, *Phys. Rev.* **D77** (2008) 074010, [hep-ph/0703207].

[30] S. Fleming, A. H. Hoang, S. Mantry, and I. W. Stewart, *Top Jets in the Peak Region: Factorization Analysis with NLL Resummation*, *Phys. Rev.* **D77** (2008) 114003, [arXiv:0711.2079].

[31] J. Alwall, R. Frederix, S. Frixione, V. Hirschi, F. Maltoni, et al., *The automated computation of tree-level and next-to-leading order differential cross sections, and their matching to parton shower simulations*, *JHEP* **1407** (2014) 079, [arXiv:1405.0301].

[32] N. Kauer and G. Passarino, *Inadequacy of zero-width approximation for a light Higgs boson signal*, *JHEP* **08** (2012) 116, [arXiv:1206.4803].

[33] N. Kauer, *Inadequacy of zero-width approximation for a light Higgs boson signal*, *Mod.Phys.Lett.* **A28** (2013) 1330015, [arXiv:1305.2092].

[34] N. Kauer, *Interference effects for $H \to WW/ZZ \to \ell\bar{\nu}_\ell\bar{\ell}\nu_\ell$ searches in gluon fusion at the LHC*, *JHEP* **12** (2013) 082, [arXiv:1310.7011].

[35] F. Caola and K. Melnikov, *Constraining the Higgs boson width with ZZ production at the LHC*, *Phys.Rev.* **D88** (2013) 054024, [arXiv:1307.4935].

[36] J. M. Campbell, R. K. Ellis, and C. Williams, *Bounding the Higgs width at the LHC using full analytic results for $gg \to e^-e^+\mu^-\mu^+$*, *JHEP* **1404** (2014) 060, [arXiv:1311.3589].

[37] J. M. Campbell, R. K. Ellis, and C. Williams, *Bounding the Higgs width at the LHC: Complementary results from $H \to WW$*, *Phys.Rev.* **D89** (2014), no. 5 053011, [arXiv:1312.1628].

[38] S. Liebler, G. Moortgat-Pick, and G. Weiglein, *Off-shell effects in Higgs processes at a linear collider and implications for the LHC*, *JHEP* **1506** (2015) 093, [arXiv:1502.07970].

[39] **LHC Higgs Cross Section Working Group** Collaboration, J. R. Andersen et al., *Handbook of LHC Higgs Cross Sections: 3. Higgs Properties*, arXiv:1307.1347.

[40] **LHC Higgs Cross Section Working Group** Collaboration, A. David et al., *LHC HXSWG interim recommendations to explore the coupling structure of a Higgs-like particle*, arXiv:1209.0040.

[41] M. Ghezzi, G. Passarino, and S. Uccirati, *Bounding the Higgs Width Using Effective Field Theory*, *PoS* **LL2014** (2014) 072, [arXiv:1405.1925].

[42] C. Englert and M. Spannowsky, *Limitations and Opportunities of Off-Shell Coupling Measurements*, *Phys. Rev.* **D90** (2014) 053003, [arXiv:1405.0285].

[43] C. Englert, Y. Soreq, and M. Spannowsky, *Off-Shell Higgs Coupling Measurements in BSM scenarios*, *JHEP* **05** (2015) 145, [arXiv:1410.5440].

[44] H. E. Logan, *Hiding a Higgs width enhancement from off-shell $gg(\to h^*) \to ZZ$ measurements*, arXiv:1412.7577.

[45] M. Jezabek and J. H. Kühn, *QCD Corrections to Semileptonic Decays of Heavy Quarks*, *Nucl. Phys.* **B314** (1989) 1.

[46] A. Czarnecki, *QCD corrections to the decay $t \to Wb$ in dimensional regularization*, *Phys. Lett.* **B252** (1990) 467–470.

[47] C. S. Li, R. J. Oakes, and T. C. Yuan, *QCD corrections to $t \to W^+ b$*, *Phys. Rev.* **D43** (1991) 3759–3762.

[48] A. Denner and T. Sack, *The Top width*, *Nucl. Phys.* **B358** (1991) 46–58.

[49] G. Eilam, R. R. Mendel, R. Migneron, and A. Soni, *Radiative corrections to top quark decay*, *Phys. Rev. Lett.* **66** (1991) 3105–3108.

[50] A. Czarnecki and K. Melnikov, *Two loop QCD corrections to top quark width*, *Nucl. Phys.* **B544** (1999) 520–531, [hep-ph/9806244].

[51] K. G. Chetyrkin, R. Harlander, T. Seidensticker, and M. Steinhauser, *Second order QCD corrections to $\Gamma(t \to Wb)$*, *Phys. Rev.* **D60** (1999) 114015, [hep-ph/9906273].

[52] J. Gao, C. S. Li, and H. X. Zhu, *Top Quark Decay at Next-to-Next-to Leading Order in QCD*, *Phys. Rev. Lett.* **110** (2013), no. 4 042001, [arXiv:1210.2808].

[53] M. Brucherseifer, F. Caola, and K. Melnikov, *$\mathcal{O}(\alpha_s^2)$ corrections to fully-differential top quark decays*, *JHEP* **04** (2013) 059, [arXiv:1301.7133].

[54] **Particle Data Group** Collaboration, K. Olive et al., *Review of Particle Physics*, *Chin.Phys.* **C38** (2014) 090001.

[55] P. Batra and T. M. Tait, *Measuring the W-t-b Interaction at the ILC*, *Phys.Rev.* **D74** (2006) 054021, [hep-ph/0606068].

[56] W. Bernreuther, P. Gonzalez, and M. Wiebusch, *The Top Quark Decay Vertex in Standard Model Extensions*, *Eur. Phys. J.* **C60** (2009) 197–211, [arXiv:0812.1643].

[57] **CDF** Collaboration, T. A. Aaltonen et al., *Direct Measurement of the Total Decay Width of the Top Quark*, *Phys. Rev. Lett.* **111** (2013), no. 20 202001, [arXiv:1308.4050].

[58] M. Beneke, Y. Kiyo, P. Marquard, A. Penin, J. Piclum, and M. Steinhauser, *Next-to-next-to-next-to-leading order QCD prediction for the top anti-top S-wave pair production cross section near threshold in e+ e- annihilation*, arXiv:1506.06864.

[59] M. Martinez and R. Miquel, *Multiparameter fits to the t anti-t threshold observables at a future e^+e^- linear collider*, *Eur. Phys. J.* **C27** (2003) 49–55, [hep-ph/0207315].

[60] T. Horiguchi, A. Ishikawa, T. Suehara, K. Fujii, Y. Sumino, Y. Kiyo, and H. Yamamoto, *Study of top quark pair production near threshold at the ILC*, arXiv:1310.0563.

[61] K. Seidel, F. Simon, M. Tesar, and S. Poss, *Top quark mass measurements at and above threshold at CLIC*, *Eur.Phys.J.* **C73** (2013), no. 8 2530, [arXiv:1303.3758].

[62] **Linear Collider ILD Concept Group -** Collaboration, T. Abe et al., *The International Large Detector: Letter of Intent*, arXiv:1006.3396.

[63] V. Hirschi, R. Frederix, S. Frixione, M. V. Garzelli, F. Maltoni, and R. Pittau, *Automation of one-loop QCD corrections*, *JHEP* **05** (2011) 044, [arXiv:1103.0621].

[64] R. Frederix, S. Frixione, F. Maltoni, and T. Stelzer, *Automation of next-to-leading order computations in QCD: The FKS subtraction*, *JHEP* **10** (2009) 003, [arXiv:0908.4272].

[65] S. Frixione, Z. Kunszt, and A. Signer, *Three jet cross-sections to next-to-leading order*, *Nucl. Phys.* **B467** (1996) 399–442, [hep-ph/9512328].

[66] A. Denner, S. Dittmaier, M. Roth, and D. Wackeroth, *Predictions for all processes $e^+e^- \to 4$ fermions $+\gamma$*, *Nucl.Phys.* **B560** (1999) 33–65, [hep-ph/9904472].

[67] A. Denner, S. Dittmaier, M. Roth, and L. Wieders, *Electroweak corrections to charged-current $e^+e^- \to 4$ fermion processes: Technical details and further results*, *Nucl.Phys.* **B724** (2005) 247–294, [hep-ph/0505042].

[68] M. Moretti, T. Ohl, and J. Reuter, *O'Mega: An Optimizing matrix element generator*, hep-ph/0102195.

[69] W. Kilian, T. Ohl, and J. Reuter, *WHIZARD: Simulating Multi-Particle Processes at LHC and ILC*, *Eur. Phys. J.* **C71** (2011) 1742, [arXiv:0708.4233].

[70] I. Garcia, M. Perello, E. Ros, and M. Vos, *Study of single top production at high energy electron positron colliders*, arXiv:1411.2355.

[71] G. Bevilacqua, M. Czakon, A. van Hameren, C. G. Papadopoulos, and M. Worek, *Complete off-shell effects in top quark pair hadroproduction with leptonic decay at next-to-leading order*, *JHEP* **02** (2011) 083, [arXiv:1012.4230].

[72] A. Denner, S. Dittmaier, S. Kallweit, and S. Pozzorini, *NLO QCD corrections to WWbb production at hadron colliders*, *Phys. Rev. Lett.* **106** (2011) 052001, [arXiv:1012.3975].

[73] A. Denner, S. Dittmaier, S. Kallweit, and S. Pozzorini, *NLO QCD corrections to off-shell top-antitop production with leptonic decays at hadron colliders*, *JHEP* **10** (2012) 110, [arXiv:1207.5018].

[74] A. S. Papanastasiou, R. Frederix, S. Frixione, V. Hirschi, and F. Maltoni, *Single-top t-channel production with off-shell and non-resonant effects*, *Phys. Lett.* **B726** (2013) 223–227, [arXiv:1305.7088].

[75] R. Frederix, *Top Quark Induced Backgrounds to Higgs Production in the $WW^{(*)} \to ll\nu\nu$ Decay Channel at Next-to-Leading-Order in QCD*, *Phys. Rev. Lett.* **112** (2014), no. 8 082002, [arXiv:1311.4893].

[76] F. Cascioli, S. Kallweit, P. Maierhöfer, and S. Pozzorini, *A unified NLO description of top-pair and associated Wt production*, *Eur. Phys. J.* **C74** (2014), no. 3 2783, [arXiv:1312.0546].

[77] M. Cacciari, G. P. Salam, and G. Soyez, *FastJet User Manual*, *Eur. Phys. J.* **C72** (2012) 1896, [arXiv:1111.6097].

[78] P. Falgari, P. Mellor, and A. Signer, *Production-decay interferences at NLO in QCD for t-channel single-top production*, *Phys. Rev.* **D82** (2010) 054028, [arXiv:1007.0893].

[79] P. Falgari, F. Giannuzzi, P. Mellor, and A. Signer, *Off-shell effects for t-channel and s-channel single-top production at NLO in QCD*, *Phys. Rev.* **D83** (2011) 094013, [arXiv:1102.5267].

[80] P. Falgari, A. Papanastasiou, and A. Signer, *Finite-width effects in unstable-particle production at hadron colliders*, *JHEP* **1305** (2013) 156, [arXiv:1303.5299].

[81] E. Devetak, A. Nomerotski, and M. Peskin, *Top quark anomalous couplings at the International Linear Collider*, *Phys. Rev.* **D84** (2011) 034029, [arXiv:1005.1756].

[82] R. G. Stuart, *Gauge invariance, analyticity and physical observables at the Z0 resonance*, *Phys.Lett.* **B262** (1991) 113–119.

[83] A. Aeppli, G. J. van Oldenborgh, and D. Wyler, *Unstable particles in one loop calculations*, *Nucl.Phys.* **B428** (1994) 126–146, [hep-ph/9312212].

[84] M. Beneke, A. P. Chapovsky, A. Signer, and G. Zanderighi, *Effective theory approach to unstable particle production*, *Phys. Rev. Lett.* **93** (2004) 011602, [hep-ph/0312331].

[85] M. Beneke, P. Falgari, C. Schwinn, A. Signer, and G. Zanderighi, *Four-fermion production near the W pair production threshold*, *Nucl. Phys.* **B792** (2008) 89–135, [arXiv:0707.0773].

[86] G. Moortgat-Pick, T. Abe, G. Alexander, B. Ananthanarayan, A. Babich, et al., *The Role of polarized positrons and electrons in revealing fundamental interactions at the linear collider*, *Phys.Rept.* **460** (2008) 131–243, [hep-ph/0507011].

[87] J. M. Campbell, R. K. Ellis, P. Nason, and E. Re, *Top-pair production and decay at NLO matched with parton showers*, *JHEP* **04** (2015) 114, [arXiv:1412.1828].

[88] T. Jeo and P. Nason, *On the Treatment of Resonances in Next-to-Leading Order Calculations Matched to a Parton Shower*, arXiv:1509.09071.